Polymer threadings and rigidity dictate the viscoelasticity of entangled ring-linear blends and their composites with rigid rod microtubules

Karthik R. Peddireddy, Ryan Clairmont and Rae M. Robertson-Anderson

Citation: Journal of Rheology **67**, 125 (2023); doi: 10.1122/8.0000529
View online: https://doi.org/10.1122/8.0000529
View Table of Contents: https://sor.scitation.org/toc/jor/67/1
Published by the The Society of Rheology

Polymer threadings and rigidity dictate the viscoelasticity of entangled ring-linear blends and their composites with rigid rod microtubules

Karthik R. Peddireddy, Ryan Clairmont, and Rae M. Robertson-Anderson[a)]

Department of Physics and Biophysics, University of San Diego, 5998 Alcala Park, San Diego, California 92110, USA

(Received 15 July 2022; final revision received 14 September 2022; published 9 November 2022)

Abstract

Mixtures of polymers of varying topologies and stiffnesses display complex emergent rheological properties that often cannot be predicted from their single-component counterparts. For example, entangled blends of ring and linear polymers have been shown to exhibit enhanced shear thinning and viscosity, as well as prolonged relaxation timescales, compared to pure solutions of rings or linear chains. These emergent properties arise in part from the synergistic threading of rings by linear polymers. Topology has also been shown to play an important role in composites of flexible (e.g., DNA) and stiff (e.g., microtubules) polymers, whereby rings promote mixing while linear polymers induce demixing and flocculation of stiff polymers, with these topology-dependent interactions giving rise to highly distinct rheological signatures. To shed light on these intriguing phenomena, we use optical tweezers microrheology to measure the linear and nonlinear rheological properties of entangled ring-linear DNA blends and their composites with rigid microtubules. We show that linear viscoelasticity is primarily dictated by microtubules at lower frequencies, but their contributions become frozen out at frequencies above the DNA entanglement rate. In the nonlinear regime, we reveal that mechanical response features, such as shear thinning and stress softening, are mediated by entropic stretching, threading, and flow alignment of entangled DNA, as well as forced dethreading, disentanglement, and clustering. The contributions of each of these mechanisms depend on the strain rate as well as the entanglement density and stiffness of the polymers, leading to nonmonotonic rate dependences of mechanical properties that are most pronounced for highly concentrated ring-linear blends rather than DNA-microtubule composites. https://doi.org/10.1122/8.0000529

I. INTRODUCTION

For decades now, ring polymers have been the subject of great fascination and frustration, not only because of their biological relevance and industrial applications, but also their simple yet unique "endless" topology. Theories describing the dynamics of entangled linear polymers, based on the well-established tube model introduced by de Gennes and advanced by Doi and Edwards, rely heavily on the free ends of linear chains [1,2]. Reptation, whereby an entangled polymer diffuses "head-first" in a curvilinear fashion along its confining tube of radius a, formed by the surrounding entangling polymers, is predicted to be the dominant relaxation mode for entangled linear chains, occurring over a timescale τ_D. Discrepancies between reptation theory and experiment have been rectified by including contour length fluctuations, in which the polymer ends can rapidly relax to accelerate the disengagement timescale τ_D [3–5], and constraint release, in which an entangled polymer relaxes by a very slow process of the surrounding entangling chains reptating away to release their constraints [6]

Their lack of free ends prohibits a straightforward extension of tube models to ring polymers [7,8]. Multiple theories have been proposed to describe the dynamics of entangled rings, which have been modeled as double-folded structures, akin to linear polymers, and amoebalike or pom-pom lattice animals, similar to branched polymers [7,9–13]. Entangled rings have also been predicted to display glassy dynamics due to threadings between the rings [14,15]. Experiments to test these differing models have been complicated by the near impossibility of producing samples of pure rings without linear polymer "contaminants" [16,17]. However, this issue had the important positive consequence of revealing emergent dynamics of ring-linear polymer blends [7,16,18,19]. For example, ring-linear blends have been shown to exhibit increased viscosity [16,18,20–23], slower relaxation modes [18,24,25], and more pronounced shear thinning compared to their pure ring and linear counterparts [18,24,26]. These emergent rheological properties are expected to arise, in part, from the synergistic threading of rings by linear chains [27–31], which inhibits the reptation of rings such that they relax primarily via the slower mode of constraint release. Threading events, which have been shown to be the most prevalent in blends with comparable concentrations of rings and linear chains [18,28,32], have also been shown to enhance polymer stretching and alignment along the direction of the strain, compared to their pure ring counterparts, which in turn, facilitates shear thinning and elastic Rouse-like retraction [18,20,28,32].

We previously showed that entangled ring-linear DNA blends with comparable mass fractions f of linear and ring DNA ($f_L \approx f_R$) exhibit the strongest shear thinning and largest elastic plateaus that persist over the widest frequency range [18]. This nonmonotonic dependence of viscoelastic properties on f_L persists even in the nonlinear regime in

Note: This paper is part of the special issue on Ring Polymers.

[a)]Author to whom correspondence should be addressed: randerson@sandiego.edu

which the blends are pushed far from equilibrium by strains and strain rates that are much larger than the characteristic length and time scales of the blends [18].

We also revealed that a subtle change in DNA topology–free (linear) versus connected (rings) ends had a dramatic effect on the structure and viscoelastic properties of composites of stiff microtubules (MT) polymerized in the presence of entangled linear or ring DNA [33]. Linear DNA facilitated MT polymerization and flocculation, while ring DNA hindered MT polymerization and promoted DNA-MT mixing. These distinct structural properties gave rise to emergent topology-dependent rheology, whereby the plateau modulus G_N^0 for ring composites increased monotonically with MT concentration, while G_N^0 for linear DNA composites increased dramatically with a small addition of MTs, after which G_N^0 surprisingly decreased with further increase in MT concentration [33].

The fascinating emergent rheological properties of equal mass ring-linear DNA blends ($f_L \approx f_R$) and DNA-MT composites motivate the following questions: What rheological properties will emerge in composites of microtubules and equal mass ring-linear DNA blends? What roles do ring-linear threadings, entanglements, and polymer flexibility play in the hypothesized emergent rheology?

To address these questions, we investigate the linear and nonlinear microrheological properties of entangled ring-linear blends of equal mass fraction ($f_L \approx f_R$) and their composites with microtubules [Fig. 1(a)]. The ring-linear blends are identical in composition, comprising linear and ring DNA of equal contour lengths of $L \simeq 39\ \mu$m (115 kbp) and mass fractions, but vary in overall DNA concentration ($c_D = 0.5$ mg/ml and 0.65 mg/ml). The DNA-MT composite is produced by directly polymerizing $c_T = 0.7$ mg/ml tubulin in the $c_D = 0.5$ mg/ml ring-linear DNA blend. We chose the tubulin concentration c_T such that the corresponding entanglement tube diameter d_T is comparable to that of the 0.65 mg/ml DNA blend. In this way, we can directly compare the effects of adding stiff (MTs) or flexible (DNA) polymers to a ring-linear DNA blend. As shown in Fig. 1(a), we denote these three systems by the concentrations of DNA and tubulin in mg/ml: c_D:$c_T = 0.5$:0, 0.65:0, and 0.5:0.7. We use optical tweezers microrheology to systematically compare the viscoelastic properties of the 0.5:0 DNA blend with the 0.65:0 DNA blend and 0.5:0.7 DNA-MT composite in both linear and nonlinear regimes.

We find that while the addition of either DNA or MTs to the 0.5:0 blend increases the magnitudes of the linear viscoelastic moduli and extends the longest relaxation timescale, the frequency dependence is relatively insensitive to increased DNA concentration whereas MTs significantly increase the elastic contribution to the response. Moreover, the effect of MTs on the dynamics becomes frozen out at higher frequencies in which the dynamics are dominated by the DNA. We also observe complex nonlinear force response characteristics with dependences on strain rate and network composition that are surprisingly distinct from the linear regime. Notably, both 0.5 mg/ml systems display similar nonlinear rheological features, including strain softening and reduced shear thinning, while 0.65:0 exhibits enhanced shear thinning and unique nonmonotonic rate dependences of rheological features.

To frame our results summarized above, we first describe in more detail the physical properties of DNA blends and composites that we study, as well as relevant theoretical predictions based on these properties. The contour lengths of both the ring and linear DNA are fixed at $L \simeq 39\ \mu$m (115 kbp). However, due to their end-closure, the rings have a ∼1.58× smaller radius of gyration R_G than their linear counterparts in good solvent conditions (as we have here) [34–36]. We note that this ratio $R_{G,L}/R_{G,R}$, which we empirically determined, is consistent with theoretical models for rings in good solvent conditions with appreciable excluded volume interactions. However, it is higher than that predicted for theta solvent conditions and by other models that treat excluded volume effects differently [37–39]. Specifically, we previously measured dilute-limit diffusion coefficients of $D_L = 0.3\ \mu$m^2/s and $D_R = 0.42\ \mu$m^2/s for 115 kbp linear and ring DNA, respectively, from which we compute the corresponding radii of gyration $R_{G,L} \simeq 883$ nm and $R_{G,R} \simeq 551$ nm [34]. From these values, we determine the polymer overlap concentration of the ring-linear DNA blend via $c^*_{RL}=(3/4\pi)(M/N_A)/(f_L R^3_{G,L} + f_R R^3_{G,R})$, where M is the DNA molecular weight and $f_L \simeq f_R \simeq 0.5$ [2]. Our computed value of $c^*_{RL}\simeq 71\ \mu$g/ml yields $c_{D,\downarrow} = 0.5$ mg/ml $\simeq 7c^*_{RL}$ and $c_{D,\uparrow} = 0.65$ mg/ml $\simeq 9c^*_{RL}$. For reference, the overlap concentrations for the corresponding single-topology DNA solutions are c^*_L=44 μg/ml and c^*_R=182 μg/ml.

Our previous diffusion measurements for the ring and linear DNA showed that the critical concentration for the onset of entanglement scaling for both topologies is $c_e \simeq 6c^*_L$ [40], within the range of $\sim 4c^*_L$ to $\sim 10c^*_L$ reported for DNA in other works [41–47]. Specifically, our measured c_e value is in line with those reported for DNA in Refs. 41, 43–45, 48, and 49 but are smaller than ~ 9–$10\,c^*_L$ reported from Refs. 46 and 47 in which lower-salt buffer conditions are used. We, therefore, estimate that the $c_{D,\uparrow} = 0.65$ mg/ml ($\sim 15c^*_L \simeq 2.5c_e$) solution is fully entangled while the $c_{D,\downarrow} = 0.5$ mg/ml ($\sim 11c^*_L \simeq 1.8c_e$) solution is more weakly entangled.

According to the Doi–Edwards tube model, the tube radius for entangled linear polymers is $a_L \simeq (24N_e/5)^{1/2}R_{G,L}$, where $N_e \simeq (4/5)cRT/MG^0_N$ is the number of Kuhn lengths ($l_k \simeq 100$ nm) per entanglement segment, $l_e = l_k N_e$ is the entanglement length, and G^0_N is the plateau modulus [2]. We previously measured $G^0_N \simeq 0.2$ Pa for solutions of linear DNA of lengths 11–115 kbp at concentration $c = 1$ mg/ml [18,50], comparable to G^0_N measured via bulk rheology for calf thymus DNA in Ref. 48. Using this G^0_N value and the predicted scaling relation $G^0_N \sim c^{2.25}$ for entangled linear polymer solutions in good solvent conditions [20,51], we compute $G^0_N \simeq 42$ mPa and ∼76 mPa for $c_{D,\downarrow}$ and $c_{D,\uparrow}$ linear DNA solutions, from which we can further compute N_e and a_L (Table I). We note that the 2.25 scaling exponent used to relate G^0_N to c is not exact, but rather, within a range of theoretical and empirical values of ∼2.22 to ∼2.31 reported for entangled polymers in good solvent conditions [20,51]. We further note that our measured G^0_N value of ∼0.2 Pa is lower than $G^0_N \simeq 1$ Pa reported for 1 mg/ml lambda DNA solutions

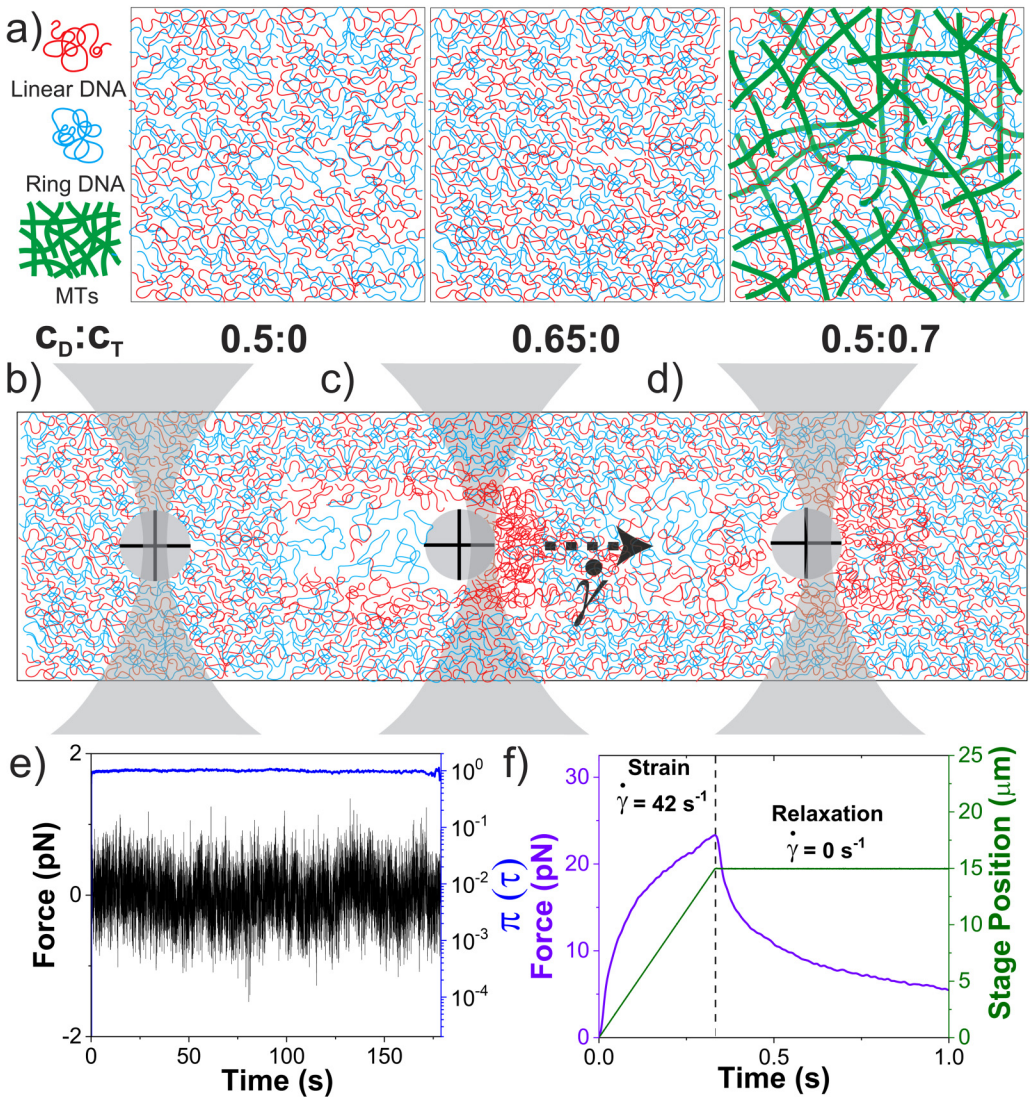

FIG. 1. Measuring the linear and nonlinear microrheological properties of entangled ring-linear DNA blends and their composites with rigid microtubules. (a) Cartoons of ring-linear DNA blends and the DNA-MT composite, defined by the mass concentrations (mg/ml) of DNA c_D (0.5 or 0.65) and tubulin c_T (0 or 0.7). (b) Cartoon of microsphere (gray circle) with radius $R = 2.25\,\mu$m, embedded in a ring-linear DNA blend and trapped using a focused Gaussian laser beam (gray). Linear microrheology measurements are performed by measuring the thermal deviations of the bead from the trap center in equilibrium. (c) For nonlinear microrheology measurements, the same optically trapped bead is displaced $15\,\mu$m ($\gamma = 3$) through the blend at logarithmically spaced speeds $v = 10$–$200\,\mu$m/s, corresponding to strain rates $\dot{\gamma} = 3v/\sqrt{2}R = 9.4$–$189\ \mathrm{s}^{-1}$. (d) The bead motion is then halted and the surrounding polymers are allowed to relax back to equilibrium. (e) Sample thermal oscillation data (black), captured for 200 s at 20 kHz, for the 0.5:0 DNA blend. From the thermal oscillations, we compute normalized mean square displacements $\pi(\tau)$ (blue) which we use to extract viscoelastic moduli using GSER (see Sec. II). (f) For nonlinear microrheology measurements, we record the stage position (green) and force exerted on the trapped bead (violet) during (0.075–1.5 s) and following (15 s) the bead displacement (delineated by dashed lines) at 20 kHz. Data shown are for the 0.5:0 DNA blend at $\dot{\gamma} = 42\ \mathrm{s}^{-1}$.

in Refs. 20 and 52. The differences between these values may be due to the lower-salt conditions used in Refs. 20 and 52 compared to our studies and those of Ref. 48. As well as inherent differences between bulk rheology and microrheology measurements, as discussed previously [53,54].

From our estimated tube radius a_L, we compute the predicted fastest relaxation timescale, i.e., the entanglement time $\tau_{e,L} = a_L^4/24R_{G,L}^2 D_L$, which is the time scale over which thermally diffusing chain segments reach the edge of the reptation tube (Table I). Similarly, we estimate the slowest predicted relaxation timescale, the disengagement time $\tau_{D,L} = 36R_{G,L}^4/\pi^2 a_L^2 D_L$, which is the time over which an entangled polymer reptates out of its initial deformed tube (Table I). To estimate the corresponding tube radius and relaxation times for the ring DNA, a_R, $\tau_{e,R}$, and $\tau_{D,R}$, we use the predicted relations from the pom-pom ring model [9], $a_R/a_L = (5N^{-0.4})^{1/2}$ and $\tau_{D,R}/\tau_{D,L} = (a_R/a_L)^2 = N^{-0.4}$, where N is the number of Kuhn lengths per chain ($N \simeq 388$ for 115 kbp DNA) (Table I).

From a_R and a_L computed for $c_{D,\downarrow}$ and $c_{D,\uparrow}$ DNA solutions (Table I), we can estimate the effective tube diameter for the $c_{D,\downarrow}$ and $c_{D,\uparrow}$ ring-linear DNA blends (i.e., 0.5:0, 0.65:0) by considering a_L and a_R values for the $f_L \simeq f_R \simeq 0.5$ fractions of linear and ring DNA in the blends, $a_{L,b}$ and $a_{R,b}$, which are at concentrations of $f_{L/R}{}^*c_{D,\downarrow} \simeq 0.25$ and $f_{L/R}{}^*c_{D,\uparrow} \simeq 0.375$ mg/ml. From the expressions and scaling relations described above, we determine $a_{L,b} \simeq 1.7$ and $a_{R,b} \simeq 1.1\,\mu$m for the $c_{D,\downarrow}$ blend and $a_{L,b} \simeq 1.1$ and

TABLE I. Predicted length and timescales for entangled 115 kbp DNA solutions and blends. Predicted values for the entanglement number N_e, entanglement length l_e, number of entanglements per chain n_e, tube radius a, entanglement time τ_e, and disengagement time τ_D for solutions of linear (rows 1 and 2) and ring (rows 3 and 4) DNA at concentrations c listed in column two. The last two rows (ring-linear) list corresponding estimates for the 0.5 ($c_{D,\downarrow}$) and 0.65 mg/ml ($c_{D,\uparrow}$) ring-linear blends examined here. Entries with – are missing values because there is no measured G_N^0 for pure ring DNA in the literature, preventing an accurate determination of l_e. Values that begin with * are estimates based on the relation $a_b \simeq (l_k l_{e,b})^{1/2}$. Italicized values are empirically determined from data shown in Fig. 2 as described in the text.

DNA topology	c (mg/ml)	N_e	l_e (μm)	$n_e = L/l_e$	a (μm)	τ_e (ms)	τ_D (s)
Linear	$c_{D,\downarrow} = 0.5$	117	11.7	3.3	1.08	241	6.2
Linear	$c_{D,\uparrow} = 0.65$	846	8.46	4.6	0.92	124	8.6
Ring	$c_{D,\downarrow} = 0.5$	–	–	–	0.73	56	0.26
Ring	$c_{D,\uparrow} = 0.65$	–	–	–	0.62	25	0.36
Ring-linear	0.25–0.25	*106	*10.6 ($l_{e,b}$)	*3.7	1.03 (a_b)	1100	39
Ring-linear	0.375–0.375	*722	*7.2 ($l_{e,b}$)	*5.4	0.85 (a_b)	390	>63

$a_{R,b} \simeq 0.95\,\mu$m for the $c_{D,\uparrow}$ blend. From these values, we estimate an effective tube radius a_b for the $c_{D,\downarrow}$ and $c_{D,\uparrow}$ blends using the relation $a_b^{-3} = [(a_{L,b})^{-3} + (a_{R,b})^{-3}]$ that considers the density of each cubic tube radius a_b^3 to arrive at values of $a_b \simeq 1.03$ and $\sim 0.85\,\mu$m for $c_{D,\downarrow}$ and $c_{D,\uparrow}$ blends, respectively [55]. The theoretical mesh size of the entangled MT network for $c_T = 0.7$ mg/ml tubulin is $\xi = 0.89 c_T^{-1/2} \simeq 1.1\,\mu$m, which is comparable to the effective tube radius a_b of the $c_{D,\uparrow}$ blend [56]. We can further estimate an effective entanglement length $l_{e,b}$ from the relation $a_b \simeq (l_k l_{e,b})^{1/2}$ which gives $l_{e,b}(c_{D,\downarrow}) \simeq 10.6$ and $l_{e,b}(c_{D,\uparrow}) \simeq 7.2\,\mu$m.

II. METHODS

A. DNA

We prepared double-stranded, 115 kilobasepair (kbp) DNA by the replication of cloned bacterial artificial chromosomes (BACs) in *Escherichia coli*, followed by extraction, purification, concentration, and resuspension in TE10 buffer [10 mm Tris-HCl (pH 8), 1 mm EDTA, 10 mm NaCl] using custom-designed protocols described and validated previously [34,57]. We used gel electrophoresis image analysis to quantify the DNA concentration and mass fractions of relaxed circular (ring) and linear topologies. Using Life Technologies E-Gel Imager and Gel Quant Express software, we determined $c \simeq 0.8$ mg/ml and $f_L \simeq f_R$. For experiments, we used two different dilutions of this stock: $c_{D,\downarrow} = 0.5$ and $c_{D,\uparrow} = 0.65$ mg/ml. More details about the physical properties of the DNA are provided in the supplementary material [92].

B. Microtubules (MT)

Unlabeled and rhodamine-labeled porcine brain tubulin (Cytoskeleton, Inc; T240, TL590M) are stored at −80 °C in single-use aliquots containing 5 mg/ml tubulin dimers with an unlabeled:labeled ratio of 9:1 in PEM100 buffer [100 mm PIPES (pH 6.8), 2 mm $MgCl_2$, 2 mm EGTA]. As previously described [33], to form DNA-MT composites, we add a concentration of $c_T = 0.7$ mg/ml tubulin dimers to the $c_{D,\downarrow} = 0.5$ mg/ml DNA blend, followed by 2 mm GTP and 10 μM Taxol to polymerize and stabilize the MTs. The formed MTs are hollow rods with a diameter $D \simeq 25$ nm comprising 13 tubulin dimers per ring [58]. Based on our previous measurements in which microtubules were polymerized under similar conditions [55,56,59,60], we expect a length distribution of ∼5 to 15 μm. The mesh size of the entangled MT network is $\xi = 0.89 c_T^{-1/2} \simeq 1.1\ \mu$m.

C. Sample preparation

We perform measurements on three different systems, which we denote by the ratio of the concentrations of DNA and tubulin in mg/ml: $c_D{:}c_T = 0.5{:}0$, 0.65:0, and 0.5:0.7. For microrheology experiments, we add a trace amount of 4.5 μm polystyrene microspheres (probes), coated with Alexa-488 BSA to prevent DNA adsorption and enable fluorescence imaging, and an oxygen scavenging system (45 μg/ml glucose, 43 μg/ml glucose oxidase, 7 μg/ml catalase, and 5 μg/ml β-mercaptoethanol) to inhibit photobleaching. Sample chambers ($20 \times 3 \times 0.1$ mm^3) are made with a microscope glass slide and coverslip, each coated with BSA to prevent adsorption of DNA, MTs and beads, and separated by a layer of double-sided tape. All samples are mixed slowly and thoroughly, using wide-bore pipette tips to prevent shearing, then introduced into sample chambers through capillary action and hermetically sealed with epoxy. For the DNA-MT composite (0.5:0.7), tubulin dimers are added immediately before flowing into the chamber, and the sample chamber is incubated at 37 °C for 2 h, resulting in repeatable and reliable tubulin polymerization in the DNA blend [33].

D. Microrheology

We use optical tweezers microrheology to determine the linear and nonlinear rheological properties of the three systems (Fig. 1) [61,62]. The optical trap, built around an Olympus IX71 epifluorescence microscope, is formed from a 1064 nm Nd:YAG fiber laser (Manlight) focused with a 60× 1.4 NA objective (Olympus). Forces exerted by the polymer networks on the trapped beads are determined by recording the laser beam deflections via a position sensing detector (Pacific Silicon Sensors) at 20 kHz. The trap is calibrated for force measurement using the Stokes drag method [63–65]. All microrheological data are recorded at 20 kHz, and at least 15 trials are conducted, each with a new microsphere in an unperturbed location. The presented data are an average of

all trials and error bars represent standard error. We detect no dependence of the trials on the experimental time over the course of each ~70 min measurement window (Fig. S1 in the supplementary material) [92], suggesting that the networks are in steady-state and thermal cleaving of DNA is negligible. Moreover, our previous work examining the time-dependent rheology of smaller rings [66] has shown that, in the absence of cleaving enzymes, the rings are stable for >4 h.

1. Linear microrheology

We determine linear viscoelastic properties from the thermal fluctuations of trapped microspheres, measured by recording the associated laser deflections for 200 s [Fig. 1(e)]. We extract the elastic modulus $G'(\omega)$ and viscous modulus $G''(\omega)$ from the thermal fluctuations using the generalized Stokes–Einstein relation (GSER) as described in Ref. 67. In brief, we compute the normalized mean-squared displacements $\left(\pi(\tau) = \langle r^2(\tau)\rangle / 2\langle r^2\rangle\right)$ of the thermal forces, averaged over all trials (Fig. S2 in the supplementary material) [92], which we convert into the Fourier domain via

$$-\omega^2\,\pi(\omega) = (1 - e^{-i\omega\tau_1})\frac{\pi(\tau_1)}{\tau_1} + \dot{\pi}_\infty e^{-i\omega t_N} + \sum_{k=2}^{N}\left(\frac{\pi_k - \pi_{k-1}}{\tau_k - \tau_{k-1}}\right)(e^{-i\omega\tau_{k-1}} - e^{-i\omega\tau_k}),$$

where τ, 1, and N represent the lag time and the first and last points of the oversampled $\pi(\tau)$. $\dot{\pi}_\infty$ is the extrapolated slope of $\pi(\tau)$ at infinity. Oversampling is done using the MATLAB function PCHIP. $\pi(\omega)$ is related to viscoelastic moduli via

$$G^*(\omega) = G'(\omega) + iG''(\omega) = \left(\frac{k}{6\pi R}\right)\left(\frac{1}{i\omega\pi(\omega)} - 1\right),$$

where R and k represent the microsphere radius and trap stiffness. From $G'(\omega)$ and $G''(\omega)$, we compute the complex viscosity $\eta^*(\omega) = [(G'(\omega))^2 + (G''(\omega))^2]^{1/2}/\omega$ and loss tangent $\tan\delta = G''(\omega)/G'(\omega)$.

2. Nonlinear microrheology

We perform nonlinear microrheology measurements by displacing a trapped microsphere embedded in the sample through a distance $x = 15\,\mu$m at logarithmically spaced speeds of $v = 10$–$200\,\mu$m/s using a piezoelectric nanopositioning stage (Mad City Laboratories) to move the sample relative to the microsphere [Fig. 1(f)]. We convert the distance to strain via $\gamma = x/2R\ (= 3.4)$ and convert speed to strain rate via $\dot{\gamma} = 3v/\sqrt{2}R\ (= 9.4 - 189\ \mathrm{s}^{-1})$ [68].

III. RESULTS AND DISCUSSION

A. Linear viscoelasticity (LVE)

We first examined the linear viscoelasticity (LVE) of the three systems, c_D:c_T = 0.5:0, 0.65:0, 0.5:0.7, by extracting the frequency-dependent elastic and viscous moduli, $G'(\omega)$ and $G''(\omega)$, from the thermal fluctuations of trapped beads [see Sec. II, Figs. 1(b), 1(e), and 2]. As shown in Fig. 2(a), both DNA blends (i.e., 0.5:0, 0.65:0) display similar frequency dependence of $G'(\omega)$ and $G''(\omega)$, indicative of modestly entangled polymers, with an entanglement regime, where $G'(\omega) > G''(\omega)$, flanked by higher and lower frequency regimes in which dissipative dynamics dominate [i.e., $G''(\omega) > G'(\omega)$]. For reference, the low (slow) and high (fast) frequencies at which $G'(\omega)$ and $G''(\omega)$ crossover, $\omega_{c,s}$ and $\omega_{c,f}$, indicate the slowest ($\omega_{c,s}$) and fastest ($\omega_{c,f}$) relaxation rates of the system, which correspond to corresponding relaxation timescales $\tau_c = 2\pi/\omega_c$. While the frequency dependence of $G'(\omega)$ and $G''(\omega)$ are similar for both DNA blends, the magnitude of the moduli and the frequency range over which $G''(\omega) > G'(\omega)$ are both larger for the higher concentration blend (0.65:0), as one may expect, given the increased entanglement density [1,2,69–71].

According to Doi–Edwards theory for linear entangled polymers [2], $\tau_{c,f}$ corresponds to the entanglement time τ_e, i.e., the time it takes for a confined polymer to "feel" its tube confinement. The corresponding frequency values for 0.5:0 and 0.65:0 are $\omega_{c,f,0.5} \simeq 5.6$ and $\omega_{c,f,0.65} \simeq 16$ rad/s, respectively, such that $\tau_{c,f,0.5} \simeq 1120$ ms and $\tau_{c,f,0.65} \simeq 393$ ms. In comparison, the theoretically predicted entanglement times for linear DNA at $c = 0.5$ and 0.65 mg/ml are $\tau_{e,0.5} \simeq 241$ and $\tau_{e,0.65} \simeq 124$ ms. Both experimental and theoretical timescales are ~2× shorter for 0.65:0 compared to 0.5:0, in line with the Doi–Edwards scaling relations $\tau_e \sim a^4 \sim l_e^2 \sim c^{-2}$. Namely, increasing polymer concentration reduces the length between entanglements l_e and the corresponding tube radius a and entanglement time τ_e. While the scaling of τ_e with c for ring-linear blends qualitatively aligns with predictions for linear polymers, the magnitudes of $\tau_{c,f,0.5}$ and $\tau_{c,f,0.65}$ are ~4× higher, suggesting a lower entanglement density (i.e., larger l_e) than their pure linear polymer counterparts. This result aligns with the general concept that ring polymers are less effective at forming entanglements than linear chains due to their lack of free ends [7,9,23,72–74].

The low (slow) crossover frequency $\omega_{c,s}$ for entangled linear polymers is predicted to correspond to the disengagement rate $\omega_D = 2\pi/\tau_D$, where the disengagement time τ_D is the time for a deformed polymer to reptate out of its entanglement tube. The predicted τ_D values for $c = 0.5$ and 0.65 mg/ml linear DNA are $\tau_{D,0.5} \simeq 6.2$ and $\tau_{D,0.65} \simeq 8.6$ s, respectively. The corresponding slow timescales for 0.5:0 and 0.65:0 blends, which we compute from measured crossover frequencies $\omega_{c,s,0.5} \simeq 0.16$ and $\omega_{c,f,0.65} \lesssim 0.1$ rad/s are $\tau_{c,s,0.5} \simeq 39$ and $\tau_{c,s,0.65} \gtrsim 63$ s. Similar to the fast timescales, the concentration dependence of $\tau_{c,s}$ aligns with theoretically predicted scaling $\tau_D \sim l_e^{-1} \sim c$, but the magnitudes differ substantially. In this case, the experimentally measured relaxation times are ~6.8× longer than the predicted timescales for entangled linear chains. This result is rather surprising given that our measured fast timescales indicate that l_e is larger in the ring-linear blends compared to their linear counterparts. Specifically, given the relations $l_e \sim (\tau_{c,f})^{1/2}$ and $l_e \sim \tau_D^{-1}$, our measured $\tau_{c,f}$ values imply that l_e for the blends is ~2× larger than for pure linear chains such that $\tau_{c,s}$ should be ~2× lower.

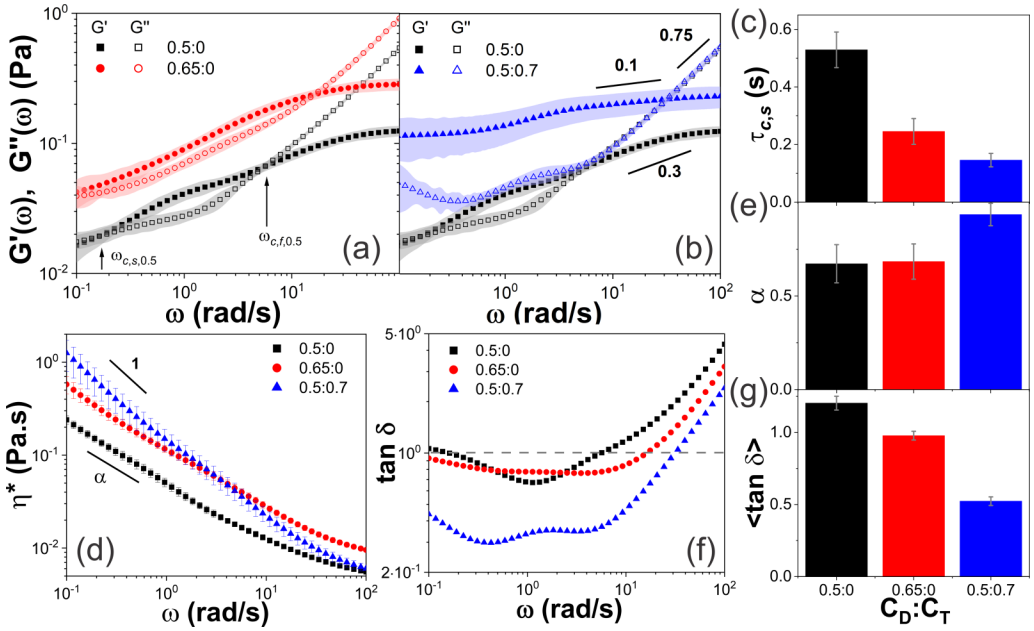

FIG. 2. Linear viscoelasticity of ring-linear DNA blends and DNA-MT composites exhibit complex dependence on polymer concentration and stiffness. [(a),(b)] Frequency-dependent elastic and viscous moduli, $G'(\omega)$ (closed symbols) and $G''(\omega)$ (open symbols) of a ring-linear DNA blend with $c_D = 0.5$ mg/ml (black) compared to (a) a higher concentration ring-linear blend ($c_D = 0.65$ mg/ml, red) and (b) its composite with microtubules polymerized from tubulin dimers of concentration $c_T = 0.7$ mg/ml (blue). The shaded region surrounding each curve represents the standard error across 15 trials. The legend demarcates each network by the ratio of DNA to tubulin concentrations c_D:c_T. Arrows point to the low (slow) and high (fast) crossover frequencies $\omega_{c,s}$ and $\omega_{c,f}$ for 0.5:0, which indicate the slowest/fastest characteristic relaxation timescales $\tau_{c,slf} = 2\pi/\omega_{c,\,slf}$ of the blend. (c) The fast relaxation timescale $\tau_{c,s}$ for 0.5:0 (black), 0.65:0 (red), and 0.5:0.7 (blue), determined from the corresponding $\omega_{c,f}$ indicates the entanglement time τ_e. (d) Complex viscosity $\eta^*(\omega)$, determined from $G'(\omega)$ and $G''(\omega)$ curves shown in (a) and (b), exhibit shear thinning $\eta^*(\omega) \sim \omega^{-\alpha}$ with (e) exponents α, computed from power-law fits to $\eta^*(0.1\text{ rad/s} < \omega < 1\text{ rad/s})$. (f) Loss tangent $\tan\delta = G''(\omega)/G'(\omega)$ versus ω computed from data shown in (a) and (b) with a dashed gray line representing $G''(\omega) = G'(\omega)$ ($\tan\delta = 1$). The frequencies at which each curve crosses the dashed line correlate with $\omega_{c,\,slf}$. (g) Frequency-averaged loss tangents $\langle\tan\delta\rangle$ for all three systems indicate the extent to which each system exhibits elastic versus viscous dynamics. $\langle\tan\delta\rangle > 1$ indicates that dissipative mechanisms dictate dynamics while $\langle\tan\delta\rangle < 1$ indicates more elastic-like dynamics with lower values indicating relatively more elasticity (less dissipation).

We can understand this substantially slower relaxation in blends by recalling that threadings between the ring and linear polymers have been shown to play a principal role in the relaxation dynamics of ring-linear blends [18,20,23,24,27–31,75–77]. Relaxation of threaded polymers has been shown to be much slower than reptation, as it relies primarily on constraint release [24,27,28,31,78,79]. Our slow relaxation timescales, which are an order of magnitude slower than theoretically predicted for linear polymers, assuming the increased entanglement length that our $\tau_{c,f}$ values indicate (i.e., ~2*6.8), are strong evidence that threading plays a dominate role in the relaxation dynamics of both DNA blends.

In Fig. 2(b), we evaluate the effect of adding microtubules to the 0.5:0 blend (i.e., c_D:$c_T = 0.5$:0.7) rather than more DNA [as in Fig. 2(a)]. Similar to increasing DNA concentration, we observe that the magnitudes of $G'(\omega)$, $G''(\omega)$, and $\omega_{c,f}$ increase when MTs are added to 0.5:0. However, unlike the 0.65:0 blend, the frequency dependence of $G'(\omega)$ for 0.5:0.7 is weaker than the 0.5:0 system. While both DNA blends roughly exhibit $G'(\omega) \sim \omega^{0.3}$ scaling [Fig. 2(a)], the 0.5:0.7 composite displays a much weaker scaling of $G'(\omega) \sim \omega^{0.1}$, akin to a rubbery plateau. We previously observed similarly weakened $G'(\omega) \sim \omega^{0.1}$ scaling for DNA-MT composites comprising either pure ring or pure linear DNA, indicating that this scaling is relatively insensitive to variations in entanglement density and threading propensity of the DNA [33]. Interestingly, this scaling is weaker than the reported $\omega^{0.17}$ scaling for pure entangled MTs at ~40% higher concentration [56]. Taken together, our results suggest that synergistic interactions between the flexible DNA and stiff MTs enhance the elasticity of the composite beyond that of their monodisperse counterparts [33]. Similar enhanced stiffness and elasticity have been reported for other composites of stiff and flexible polymers [80,81].

The viscous modulus $G''(\omega)$ is likewise larger and exhibits much weaker frequency dependence for the 0.5:0.7 composite compared to 0.5:0 over two decades of ω. This minimal ω-dependence is similar to that reported for pure MTs at 1 mg/ml over a similar frequency range [56]. However, for $\omega > \omega_{c,f,0.5}$, $G''(\omega)$ for both systems, with and without MTs, collapse to a single curve with increased ω-dependence [$G''(\omega) \sim \omega^{3/4}$]. This collapse along with similar high-ω scaling for 0.65:0 [Fig. 2(a)] and minimal ω dependence for pure MT solutions [56] suggests that the DNA dynamics dominate the viscoelasticity for timescales shorter than the entanglement time τ_e of the DNA. At these short timescales (high frequencies), the dynamics are largely dissipative as the DNA polymers do not feel their entanglement constraints. Moreover, the prohibitively slow relaxation timescales for MTs prevent appreciable contribution to the dynamics [82].

We more closely examine this high frequency regime by comparing the fast crossover frequencies $\omega_{c,f}$ for 0.5:0 and 0.5:0.7, which we measure to be $\omega_{c,f,0.5} \simeq 5.6$ and

$\omega_{c,f,0.5:0.7} \simeq 31$ rad/s, respectively. As such, while the viscous contribution to the dynamics of both systems is identical for $\omega \gtrsim 10$ rad/s, as discussed above, the onset of entanglement dynamics and elastic contributions appears to occur at ~5.6× shorter timescales for 0.5:0.7 compared to 0.5:0. Namely, the fast relaxation timescales, which we understand to be indicative of the entanglement time τ_e, are $\tau_{c,f,0.5:0} \simeq 1.1$ and $\tau_{c,f,0.5:0.7} \simeq 0.20$ s for the DNA blend and DNA-MT composite, respectively. $\tau_{c,f,0.5:0.7}$ is also nearly ~2-fold shorter than that for the 0.65:0 blend. This shorter timescale suggests that the presence of rigid MTs increases the effective entanglement density of the DNA blend more than the presence of more DNA. Finally, we note that the DNA-MT composite does not exhibit a low-ω crossover suggesting that disengagement processes are slowed substantially by the presence of rigid MTs which, themselves, have relaxation timescales that can span minutes to hours [56,82].

To further elucidate the differences in the viscoelastic properties between the three networks, we compare their respective complex viscosities $\eta^*(\omega)$ [Fig. 2(d)]. To understand the trends shown in Fig. 2(d), we first note that entangled polymers typically exhibit shear thinning, in which systems that obey the Cox–Merz rule follow $\eta^*(\omega) \sim \omega^{-\alpha}$ scaling with $0 \leq \alpha \leq 1$ [2,83–85]. This behavior is expected to be a result of the flow alignment of polymers and reaches a maximum of $\alpha \simeq 1$ for highly entangled polymer solutions and gels [2,20,26,63,85–87]. Entangled DNA solutions and blends have been reported to display weaker thinning of $\alpha \simeq 0.4 - 0.7$, largely insensitive to DNA concentration, but exhibiting maximal thinning for equal mass ring-linear blends and weakest thinning for pure rings [18,20,26,33,85]. Shear thinning is clearly evident for all three systems, with both DNA systems (0.5:0, 0.65:0) following similar scaling of $\alpha \simeq 0.65$ and the 0.5:0.7 composite obeying $\alpha \simeq 1$ for all but the highest frequencies in which the thinning of all systems is slightly weaker. This onset of weakened high-ω thinning, which indicates that the polymers do not have time to align with the flow, appears to be $\sim\omega_{c,f}$. As described above, entanglements, which mediate viscosity thinning, have a negligible role in dynamics for $\omega > \omega_{c,f}$.

Comparing the magnitudes of $\eta^*(\omega)$ across the networks ($\eta^*_{0.65}$, $\eta^*_{0.5}$, $\eta^*_{0.5:0.7}$), we observe that $\eta^*_{0.65}$ is ~2.3-fold larger than $\eta^*_{0.5}$ across the entire frequency range, similar to the corresponding $G'(\omega)$ and $G''(\omega)$ curves, and as expected, given the comparatively higher concentration and thus shorter entanglement length l_e of 0.65:0. Intriguingly, we find that for low frequencies ($\omega \lesssim 3$ rad/s), the DNA-MT viscosity ($\eta^*_{0.5:0.7}$) is ~2× and ~4× larger than $\eta^*_{0.65}$ and $\eta^*_{0.5}$, respectively, indicating substantially increased resistance to flow; however, $\eta^*_{0.5:0.7}$ drops below $\eta^*_{0.65}$ at higher frequencies. In fact, at the highest frequencies $\eta^*_{0.5:0.7}$ is comparable to $\eta^*_{0.5}$, indicating that the microtubules do not contribute significantly to the viscoelastic response in the high-ω limit. We can understand this short-timescale phenomenon as arising from the coupled effects of the DNA not having enough time to feel their tube constraints formed by the entangling microtubules ($t < \tau_e$) and the microtubules not having time to appreciably relax. In other words, the contribution of the microtubules to the viscoelastic response becomes increasingly "frozen out" at sufficiently high frequencies.

The results described above and in Figs. 2(a)–2(d) indicate that the different networks undergo varying degrees of dissipation versus storage, which we quantify by the loss tangent $\tan\delta = G''(\omega)/G'(\omega)$ [Fig. 2(f)]. For reference, elastic processes dominate the response when $\tan\delta < 1$, with lower values indicating increasing elasticity; while $\tan\delta > 1$ indicates that dissipation dominates the response with higher values indicating relatively more dissipation. The frequencies at which $\tan\delta = 1$ demarcate the crossover frequencies, $\omega_{c,s}$ and $\omega_{c,f}$, discussed above. As shown, the DNA-MT composite is substantially more elastic than the DNA blends, which show similar $\tan\delta$ values between them [Figs. 2(f) and 2(g)], but the effect of MTs is more subdued at higher frequencies where $\tan\delta > 1$. The frequencies at which $\tan\delta = 1$, which align with the values we report above for $\omega_{c,f,0.5}$, $\omega_{c,f,0.65}$, and $\omega_{c,f,0.5:0.7}$, show that adding either DNA or MTs to the 0.5:0 blend extends the timescale of the elastic-like entanglement regime (i.e., where $\tan\delta < 1$). However, adding stiff MTs extends the entanglement regime over longer timescales than adding more flexible DNA ($\omega_{c,f,0.5:0.7} > \omega_{c,f,0.65}$, $\omega_{c,s,0.5:0.7} < \omega_{c,s,0.65}$), and likewise, suppresses the dissipative contributions to the entanglement regime by a factor of ~2.

Our collective linear microrheology results reveal that the addition of either DNA or MTs to the 0.5:0 DNA blend, increases the magnitudes of the viscoelastic moduli [$G'(\omega)$, $G''(\omega)$, $\eta^*(\omega)$] and extends the entanglement regime by increasing $\omega_{c,f}$ and decreasing $\omega_{c,s}$. However, increased DNA has minimal effect on the frequency dependence of the moduli, suggesting that similar mechanisms dictate the dynamics in both DNA blends. In contrast, MTs substantially weaken the frequency dependence of $G'(\omega)$, increase the degree of viscosity thinning, and decrease the loss tangent, all indicators of increased elasticity and rigidity. Notably, these effects that emerge in the 0.5:0.7 composite are frozen out at higher frequencies that are faster than the DNA entanglement rate (τ_e^{-1}) and the fastest relaxation rate of the MTs.

B. Nonlinear viscoelastic response

We next seek to determine the extent to which LVE features and mechanisms described above are preserved in the nonlinear regime in which we subject the polymers to large strains γ and fast strain rates $\dot{\gamma}$ [Figs. 1(c), 1(f), 3, and S1 in the supplementary material] [92]. As described in Methods and Fig. 1, to impart nonlinear strains, we drive the same optically trapped microspheres that we use to measure linear viscoelasticity through a strain of $\gamma = 3$ at logarithmically spaced rates of $\dot{\gamma} = 9.4 - 189\ \mathrm{s}^{-1}$ (Fig. 3) while measuring the force that the network exerts on the moving probe. To understand the force response curves shown in Figs. 3(a) and 3(b) and S1 in the supplementary material [92], we first recall that for a purely elastic material, $F(\gamma, \dot{\gamma}) \sim \gamma \sim \dot{\gamma}^0$ such that F should increase linearly with γ with a $\dot{\gamma}$-independent slope that indicates the network stiffness $K = dF/d\gamma$. Conversely, for a purely viscous solution, $F(\gamma, \dot{\gamma}) \sim \gamma^0 \sim \dot{\gamma}$ such that F should immediately rise to a

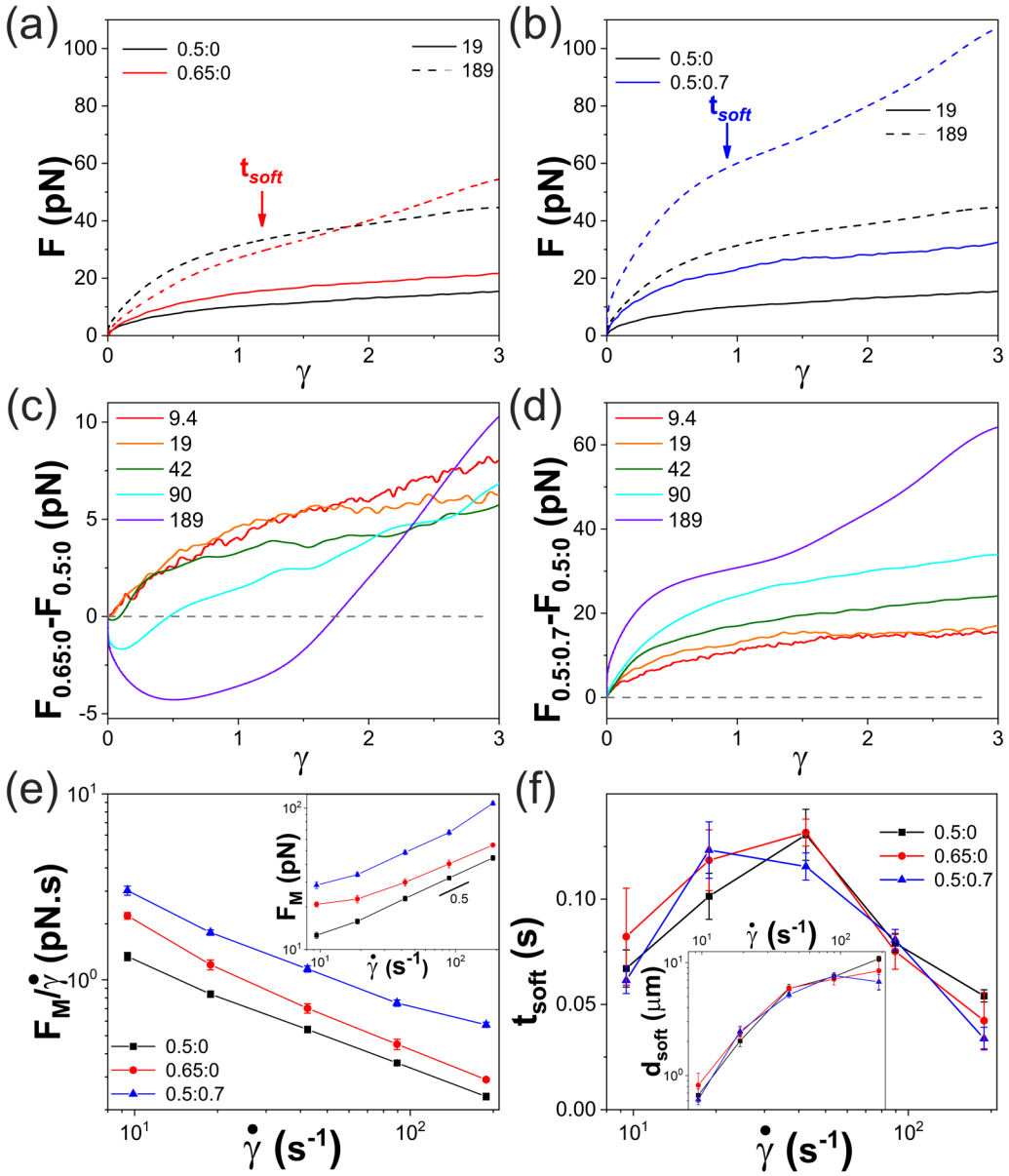

FIG. 3. The nonlinear force response reveals unique nonlinear viscoelasticity for highly entangled DNA blends (0.65:0) dictated by ring-linear threadings. [(a),(b)] Measured force F in response to nonlinear strain with rates of $\dot{\gamma} = 19\ s^{-1}$ (solid) and $189\ s^{-1}$ (dashed), as denoted in the legend, for a ring-linear DNA blend with $c_D = 0.5$ mg/ml (0.5:0, black) compared to (a) a higher concentration ring-linear blend ($c_D = 0.65$ mg/ml, red) and (b) its composite with microtubules polymerized from tubulin dimers of concentration $c_T = 0.7$ mg/ml (blue). Data for all strain rates are shown in Fig S3. [(c),(d)] The force response of the 0.5:0 blend, $F_{0.5:0}$, subtracted from the corresponding force curves for (c) 0.65:0 ($F_{0.65:0}$) and (d) 0.5:0.7 ($F_{0.65:0}$) for all strain rates $\dot{\gamma}$ (listed in the legend in s^{-1}) show markedly different effects of adding more DNA (c) versus MTs (d) to the 0.5:0 DNA blend. (e) The effective nonlinear viscosity $\eta_{en}(\dot{\gamma})$, computed by dividing the maximum force F_M reached at the end of the strain (see inset) by the strain rate $\dot{\gamma}$, for 0.5:0 (black), 0.65:0 (red), and 0.5:0.7 (blue) demonstrates nonlinear shear thinning behavior that is distinct from the linear regime. Black line in the inset, representing power-law scaling of $F_M \sim \dot{\gamma}^{0.5}$, indicates viscoelastic behavior in between purely elastic ($F_M \sim \dot{\gamma}^0$) and viscous ($F_M \sim \dot{\gamma}^1$) scaling. (f) The softening timescale t_{soft}, indicated by arrows in (a) and (b), and lengthscale d_{soft} (inset), quantify the time and lengthscales at which the force response transitions from the initial stiffer regime to the eventual softer regime, respectively. t_{soft} and d_{soft} are plotted versus $\dot{\gamma}$ for all three systems as indicated in the legend.

maximum γ-independent plateau with a magnitude that scales linearly with $\dot{\gamma}$. Figure 3 shows that all three networks generally exhibit an initial steep rise in force before rolling over to a "softer" regime with a roughly constant positive slope that is weaker than that of the initial rise. Furthermore, the maximum force F_{max} that each network exerts during strain increases monotonically with increasing $\dot{\gamma}$ [Fig. 3(e), inset]. However, as we describe below, the magnitudes and slopes of $F(\gamma, \dot{\gamma})$ in the initial "stiff" and subsequent "soft" regimes, and the time and strain distance at which the rollover to the soft regime occurs (t_{soft} and d_{soft}), all depend on the network composition and strain rate.

Comparing the nonlinear response of the two DNA blends (0.5:0, 0.65:0), we observe that, for a slow strain rate of $\dot{\gamma} = 19\ s^{-1}$, the shape of the curves for both networks are similar, but 0.65:0 exhibits a substantially stronger resistive force for the entire strain $\langle F_{0.65} \rangle \simeq 1.5 \langle F_{0.5} \rangle$, as we may expect given the increased entanglement density and linear viscoelasticity. However, for a 10× faster strain of $\dot{\gamma} = 189\ s^{-1}$, the γ-dependence of $F(\gamma)$ differs substantially

between the networks. Namely, 0.65:0 exhibits a more solid-like response with a weaker initial rise in $F(\gamma)$ and steeper "soft" regime compared to 0.5:0, suggesting that different mechanisms drive the nonlinear response of 0.65:0 versus 0.5:0. Moreover, the initial force response of 0.65:0 is surprisingly smaller than 0.5:0 and only becomes larger at $\gamma \geq 1.7$. To better quantify and examine this intriguing behavior and its dependence on strain rate, we plot the difference of the force curves for 0.65:0 and 0.5:0, $F_{0.65} - F_{0.5}$, as a function of γ for all strain rates [Fig. 3(c)]. Negative values indicate that the force response of the 0.65:0 blend ($F_{0.65}$) is (counterintuitively) lower than that of 0.5:0. As shown, this crossover behavior also manifests for $\dot{\gamma} = 90$ and 42 s^{-1} with the magnitude of the difference and the strain over which it persists decreasing with decreasing $\dot{\gamma}$.

To understand this intriguing behavior, we turn to previous optical tweezers microrheology studies that reported evidence of polymer build-up at the leading edge of the probe as well as strain-induced dethreading and alignment with flow [18,88]. In these studies, higher concentration ring-linear DNA blends displayed increased flow alignment, facilitated by threading events, which manifested as more pronounced nonlinear shear thinning. At lower concentrations, in which blends had fewer entanglements and threading events, the moving probe could dethread and disentangle polymers, allowing them to preferentially accumulate at the leading edge, rather than aligning with the strain. This build-up led to reduced shear thinning. Our results are consistent with these previous findings and elucidate the force response that these different mechanisms give rise to. At higher strain rates, DNA polymers in the 0.65:0 blend remain constrained by entanglements and threadings such that they are stretched along the strain path, leading to an elastic-like force response ($F \sim \gamma$) over much of the strain, with lower initial F values compared to 0.5:0 due to the lack of polymer build-up and the minimal stretching and alignment that occurs at these shorter lengthscales. At lower strain rates, the polymers have more time to disentangle and/or dethread in response to the moving probe, allowing polymers to more easily build-up in front of the probe, such that the strain dependence of the force response more closely resembles that of the lower concentration DNA blend. This physical description is further corroborated by recent simulations and extensional flow experiments [75] on synthetic ring-linear polymer blends that showed that ring-linear threading enhanced the flow alignment and entropic stretching of both rings and linear chains.

We observe very different effects when adding MTs to 0.5:0 compared to adding more DNA. As shown in Fig. 3(b), $F_{0.5:0.7}$ is significantly larger than $F_{0.5}$ over the entire strain for both low and high strain rates, but the shapes of the curves are similar, suggesting similar mechanisms driving the nonlinear response. This effect can be seen more clearly in Fig. 3(d) which shows that $F_{0.5:0.7} - F_{0.5}$ curves are positive for all γ and $\dot{\gamma}$ and larger in magnitude than the corresponding difference curves for the two DNA blends [Fig. 3(c)]. The steep initial rise in force for both systems, followed by a weak strain dependence, is suggestive of polymer build-up at the leading edge of the probe, as we describe above. However, at faster strain rates, the 0.5:0.7 composite exhibits stronger strain dependence, indicative of increased elasticity, as we see in the linear regime. The rigid and slow MTs provide substantially more resistance to strain than more DNA as they are unable to affinely reorient and stretch on the timescale of the nonlinear strains, with rates that are nearly all faster than the frequency range we examine in LVE measurements ($\omega = 2\pi\dot{\gamma} \simeq 60 - 1190$ rad/s). Furthermore, the rigid MT scaffold prevents the entangling DNA from stretching and aligning with the flow, instead facilitating strain-induced disentanglement and build-up at the leading edge.

To more quantitatively compare the $\dot{\gamma}$-dependence of the nonlinear force response of all three networks, we plot the corresponding maximum force F_{max} reached during the strain and effective nonlinear viscosity $\eta_{en} = F_{max}/\dot{\gamma}$, both as functions of $\dot{\gamma}$ [Fig. 3(e)]. Corroborating the trends shown in Figs. 3(a) and 3(b), we find that F_{max} for the DNA-MT composite (0.5:0.7) is ~3-fold larger than F_{max} for 0.5:0 across all strain rates, with both data sets increasing monotonically with $\dot{\gamma}$ with similar power-law scaling of $F_{max} \sim \dot{\gamma}^{0.45}$. F_{max} for 0.65:0 falls in between $F_{max,0.5:0.7}$ and $F_{max,0.5:0}$ for all $\dot{\gamma}$ but displays a weaker increase with $\dot{\gamma}$ (~0.34).

Sublinear scaling of F_{max} with $\dot{\gamma}$ is indicative of nonlinear shear thinning, which we evaluate by considering the power-law scaling of $\eta_{en} \sim \dot{\gamma}^{-\beta}$, where β is the nonlinear analog to α [Fig. 2(e)]. We find β values of $\beta_{0.5:0} \simeq 0.56 \pm 0.01$, $\beta_{0.65:0} \simeq 0.66 \pm 0.02$, and $\beta_{0.5:0.7} \simeq 0.53 \pm 0.04$ for 0.5:0, 0.65:0 and 0.5:0.7, respectively. We first note that $\beta_{0.5:0} \simeq \beta_{0.5:0.7}$ with values that are lower than their corresponding linear regime thinning exponents, suggesting, as described above, that similar mechanisms drive the nonlinear stress response of both 0.5 systems. Weaker thinning suggests reduced flow alignment which likely arises from the faster strain rates which facilitate the disentanglement and dethreading of DNA and hinder the ability of MTs to reorient and align with the strain, both effects suppressing shear thinning and promoting build-up. At first glance, these results appear at odds with our LVE measurements in which the 0.5:0.7 composite displays much stronger thinning than 0.5:0. However, as we describe in the preceding section, this enhanced thinning of the DNA-MT composite becomes weaker with increasing ω, eventually overlapping with that of 0.5:0 at frequencies comparable to the lowest nonlinear strain rate where MT contributions are largely frozen out.

We now return to the early-time strain dependence for the different networks, most clearly seen in Figs. 3(a) and 3(c), which show that the time, t_{soft}, and lengthscale, $d_{soft} = vt_{soft}$, at which $F(\gamma, \dot{\gamma})$ rolls over from the initial "stiff" regime to the subsequent "soft" regime are strongly dependent on $\dot{\gamma}$. As shown in Fig. 3(f), t_{soft} and d_{soft} are both largely insensitive to network composition, but t_{soft} exhibits a surprising nonmonotonic dependence on $\dot{\gamma}$, reaching a maximum at $\dot{\gamma} = 42$ s^{-1}. Previous differential dynamic microscopy measurements on similar systems [89] reported that flow alignment and entropic stretching of DNA followed an analogous nonmonotonic $\dot{\gamma}$ dependence that peaked at $\dot{\gamma} = 42$ s^{-1}. We can understand this nonmonotonic trend by considering that for rates below this "resonant" rate, the polymers have time

to relax and disentangle (dissipative processes) to facilitate transitioning to a softer, more fluidlike regime. Rates above this resonance are too fast for the polymers to effectively stretch and align with the flow, and instead, the moving probe forces disentanglement and dethreading. This effect is also in line with the flow-induced threading–unthreading transition reported for entangled ring-linear polystyrene blends [32,75].

By scaling t_{soft} by the strain speed v, we show that the softening lengthscale d_{soft} undergoes an initial steep increase with increasing $\dot{\gamma}$ which largely plateaus for $\dot{\gamma} \geq 42\ s^{-1}$. The average d_{soft} values in this plateau regime are $d_{soft} = 8.1 \pm 2.5$, 7.2 ± 1.3, and $6.6 \pm 1.3\ \mu m$ for 0.5:0, 0.65:0, and 0.5:0.7, respectively. Notably, these lengthscales are comparable to but slightly lower than theoretically predicted values for the entanglement lengths $l_{e,0.5:0} \simeq 11.7$ and $l_{e,0.65:0} \simeq 8.5\ \mu m$ of the DNA solutions. This agreement indicates that softening to a more dissipative regime occurs after the polymers have been entropically stretched to their maximum length set by the confining entanglements. Beyond l_e, the polymers are prohibited from stretching further and, thus, undergo dissipative processes such as disentanglement, reptation, and constraint release.

While d_{soft} and t_{soft} are largely insensitive to network composition, there are clear differences between the slopes and curvatures of the force curves for each system in both the "stiff" and "soft" regimes. To quantify these variations, we compute an effective differential modulus or stiffness, $K(\gamma) = dF/d\gamma$, where $K = 0$ for a purely viscous system (Fig. 4). As shown in Figs. 4(a)–4(c), for all systems and strain rates, $K(\gamma)$ decays monotonically from a maximum initial value K_i to a strain-independent plateau K_f with a much lower stiffness value, indicating the "soft" regime. The two 0.5 mg/ml DNA systems [Figs. 4(a) and 4(c)] show similar steady monotonic increases in stiffness with increasing $\dot{\gamma}$, with 0.5:0.7 exhibiting ~2-fold larger values for each strain rate. This trend, which can also be seen in Fig. 4(d) in which we plot K_i vs $\dot{\gamma}$ for all three systems, corroborates the physical picture that the resistance exerted by both 0.5 mg/ml systems in the nonlinear regime arises primarily from polymer build-up rather than entropic stretching. As $\dot{\gamma}$ increases, the DNA cannot as easily disentangle (a dissipative process) so the elastic contribution to the nonlinear force response (measured by K) is stronger. The increased stiffness for the 0.5:0.7 system compared to 0.5:0 can be understood simply as the contribution of the stiffer microtubules that are unable to undergo dissipative processes on the timescale of the strain.

Notably, the 0.65:0 blend exhibits starkly different behavior, including much weaker and nonmonotonic dependence of $K(\gamma)$ on strain rate as well as lower stiffness values than either of the 0.5 mg/ml systems in the initial "stiff" regime [Figs. 4(b) and 4(d)]. This effect clearly indicates that different physical phenomena underlie the nonlinear stress response for 0.65:0 compared to 0.5:0 and 0.5:0.7, as our Fig. 3 results indicate. Reduced stiffness and lack of increase with $\dot{\gamma}$ are in line with the enhanced DNA flow alignment and shear thinning, which we postulate are facilitated by ring-linear threading [18,20,26,29,75,90]. Namely, polymers become increasingly stretched and aligned along the strain path as $\dot{\gamma}$ increases, which reduces the entanglement density and, thus, stiffness.

However, as seen in the insets of Figs. 4(a)–4(c), these trends do not hold in the "soft" regime in which all systems display lower strain-independent K values that increase monotonically with $\dot{\gamma}$, suggesting that different mechanisms dictate these different regimes. As most clearly seen in Fig. 4(e), which shows the strain-averaged stiffness values in this final plateau regime K_f, the 0.65:0 blend tracks closely with the 0.5:0.7 composite while the 0.5:0 blend shows lower stiffness values and weaker $\dot{\gamma}$ dependence. This result corroborates that the force response in this softer regime is dominated by dissipative processes such as disentanglement, dethreading, and reorienting, and that the system with the weakest constraints (0.5:0) is most easily able to dissipate stress. Conversely, 0.65:0 and 0.5:0.7 retain more stiffness due to long-lived threading constraints and microtubule rigidity, respectively, both of which hinder dissipative relaxation on the timescales of the nonlinear strains.

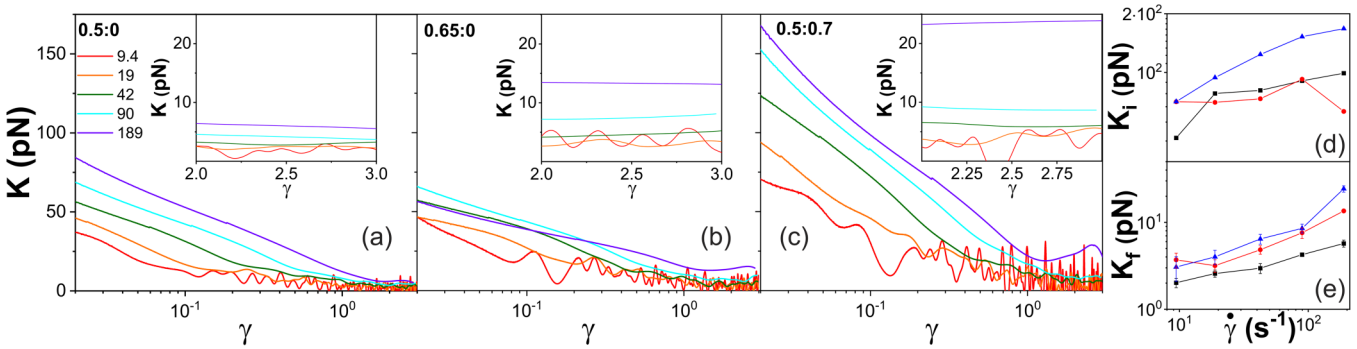

FIG. 4. The stiffness of ring-linear polymer blends and composites exhibits surprising dependence on network composition and strain rate. (a)–(c) The effective differential modulus or stiffness $K(\gamma) = dF/d\gamma$, a measure of how elastic-like or stiff each system is, plotted versus strain γ for strain rates $\dot{\gamma}$ (s^{-1}) listed in the legend for (a) 0.5:0, (b) 0.65:0, and (c) 0.5:0.7. $K(\gamma)$ for all three systems decreases from a maximum initial value K_i (plotted in d) to a nonzero plateau, amplified in the corresponding inset, with a strain-averaged value K_f [plotted in (e)]. We denote the region over which K decreases as the "stiff" regime and the terminal plateau as the "soft" regime. (d) While the initial stiffness K_i steadily increases with increasing strain rate $\dot{\gamma}$ for 0.5:0 (black) and 0.5:0.7 (blue), it exhibits a nonmonotonic dependence for 0.65:0 (red). (e) The strain-averaged stiffness in the soft regime K_f generally increases with increasing $\dot{\gamma}$ for all systems, but the magnitude and degree of increase depend on the system composition [0.5:0 (black), 0.65:0 (red), or 0.5:0.7 (blue)].

IV. CONCLUSIONS

Here, we present comprehensive linear and nonlinear microrheology measurements of entangled blends of ring and linear DNA and their composites with microtubules. We judiciously chose these systems to shed light on the highly debated roles that polymer threadings and entanglements play in the rheological properties of ring-linear polymer blends, and the extent to which these synergistic topological interactions can mediate the rheology of composites of flexible and stiff polymers. Moreover, we sought to elucidate the intriguing emergent mechanical properties that mixtures of polymers of varying topologies and stiffnesses have been shown to exhibit [32,33,75,80,91], many of which cannot be predicted from the properties of the constituents or reproduced in single-constituent systems.

As previous studies have demonstrated that threading of rings by linear chains is most pervasive in entangled blends with comparable concentrations of rings and linear chains [18,28,32], we focus our studies on blends with equal mass fractions f of ring and linear DNA ($f_R \simeq f_L \simeq 0.5$). Moreover, the surprisingly large effect that DNA topology (ring vs linear) has on the emergent rheological properties of DNA-MT composites [33] and other mixed polymer systems [79] motivates our incorporation of microtubules into ring-linear blends. Finally, we purposefully design the three networks we study here, defined by the concentrations of DNA and tubulin (c_D:c_T = 0.5:0, 0.65:0, 0.5:0.7), to have relatively modest differences in their composition, with a 30% difference in concentration between the two DNA blends (0.5:0, 0.65:0) and similar mesh sizes for the DNA-MT composite (0.5:0.7) and concentrated ring-linear blend (0.65:0). In this way, we can confidently attribute the robust variations in rheological properties we observe to modulations in the interactions between the polymers, rather than largescale structural differences.

We find that in the linear viscoelastic regime, relaxation modes are dictated by the presence of rings and threading events which prolong fast and slow relaxation timescales, respectively. However, microtubules are required to substantially augment the degree of elasticity and shear thinning of blends, with both effects becoming frozen out at high frequencies due to the slow intrinsic relaxation modes of the microtubules. Moreover, while linear rheological properties of the DNA-MT composite display markedly different frequency-dependences compared to the DNA blends, in the nonlinear regime, it is the higher concentration DNA blend (0.65:0) that displays a rate dependence that is distinct from that of the two 0.5 mg/ml systems. The distinct nonlinear features of 0.65:0 include enhanced shear thinning and reduced stiffness that displays a nonmonotonic rate dependence, and dynamics that transition from being akin to 0.5:0 at the lowest rates to 0.5:0.7 at the fastest rates. Our collective results suggest that these emergent rheological properties arise from the coupled effects of strain-induced flow alignment, dethreading, disentanglement, and build-up at the leading edge of the moving probe—all of which contribute to varying degrees, and over different timescales, in the various networks.

Our results are broadly applicable to understanding the rheological properties of diverse entangled polymeric systems, in particular, those that include "endless" ring polymers, polymers of varying stiffnesses, and mixtures thereof. These materials, which continue to fascinate and frustrate polymer scientists, are also ubiquitous in biology (e.g., cells, nucleus, cytoskeleton, mucus, cartilage) and industrial applications (e.g., flow regulation, super absorption, miscibility, adhesion), making understanding their mechanical properties of broad interest and importance.

ACKNOWLEDGMENTS

We acknowledge funding from the Air Force Office of Scientific Research Awards (Nos. FA9550-17-1-0249 and FA9550-21-1-0361) to RMRA.

AUTHOR DECLARATIONS

Conflict of Interest

The authors have no conflicts to disclose.

REFERENCES

[1] de Gennes, P. G., *Scaling Concepts in Polymer Physics* (Cornell University, Ithaca, 1979).
[2] Doi, M., and S. F. Edwards, *The Theory of Polymer Dynamics* (Oxford University, New York, 1988), Vol. 73.
[3] Doi, M., "Explanation for the 3.4-power law for viscosity of polymeric liquids on the basis of the tube model," J. Polym. Sci. Polym. Phys. Ed. **21**, 667–684 (1983).
[4] O'Connor, N. P. T., and R. C. Ball, "Confirmation of the Doi-Edwards model," Macromolecules **25**, 5677–5682 (1992).
[5] Milner, S. T., and T. C. B. McLeish, "Reptation and contour-length fluctuations in melts of linear polymers," Phys. Rev. Lett. **81**, 725–728 (1998).
[6] Graessley, W., "The constraint release concept in polymer rheology," Adv. Polym. Sci. **47**, 68–117 (1982).
[7] Richter, D., S. Goossen, and A. Wischnewski, "Celebrating soft matter's 10th anniversary: Topology matters: Structure and dynamics of ring polymers," Soft Matter **11**, 8535–8549 (2015).
[8] McLeish, T., "Polymer dynamics: Floored by the rings," Nat. Mater. **7**, 933–935 (2008).
[9] Iyer, B. V. S., A. K. Lele, and V. A. Juvekar, "Flexible ring polymers in an obstacle environment: Molecular theory of linear viscoelasticity," Phys. Rev. E **74**, 021805 (2006).
[10] Rubinstein, M., "Dynamics of ring polymers in the presence of fixed obstacles," Phys. Rev. Lett. **57**, 3023–3026 (1986).
[11] Obukhov, S. P., M. Rubinstein, and T. Duke, "Dynamics of a ring polymer in a gel," Phys. Rev. Lett. **73**, 1263–1266 (1994).
[12] Klein, J., "Dynamics of entangled linear, branched, and cyclic polymers," Macromolecules **19**, 105–118 (1986).
[13] Grosberg, A. Y., S. K. Nechaev, and E. I. Shakhnovich, "The role of topological constraints in the kinetics of collapse of macromolecules," J. Phys. **49**, 2095–2100 (1988).
[14] Lee, E., S. Kim, and Y. Jung, "Slowing down of ring polymer diffusion caused by inter-ring threading," Macromol. Rapid Commun. **36**, 1115–1121 (2015).
[15] Michieletto, D., and M. S. Turner, "A topologically driven glass in ring polymers," Proc. Natl. Acad. Sci. U.S.A. **113**, 5195–5200 (2016).

[16] Vlassopoulos, D., R. Pasquino, and F. Snijkers, "Progress in the rheology of cyclic polymers," in *Topological Polymer Chemistry Progress of Cyclic Polymers in Syntheses, Properties and Functions* (World Scientific, Singapore,2013), Ch. 14, pp. 291–316.

[17] Molnar, K., C. A. Helfer, G. Kaszas, E. Krisch, D. Chen, G. B. McKenna, J. A. Kornfield, and J. E. Puskas, "Liquid chromatography at critical conditions (LCCC): Capabilities and limitations for polymer analysis," J. Mol. Liq. **322**, 114956 (2021).

[18] Peddireddy, K. R., M. Lee, C. M. Schroeder, and R. M. Robertson-Anderson, "Viscoelastic properties of ring-linear DNA blends exhibit nonmonotonic dependence on blend composition," Phys. Rev. Res. **2**, 023213 (2020).

[19] Kapnistos, M., M. Lang, D. Vlassopoulos, W. Pyckhout-Hintzen, D. Richter, D. Cho, T. Chang, and M. Rubinstein, "Unexpected power-law stress relaxation of entangled ring polymers," Nat. Mater. **7**, 997–1002 (2008).

[20] Kong, D, S. Banik, M. J. San Francisco, M. Lee, R. M. R. Anderson, C. M. Schroeder, and G. B. McKenna, "Rheology of entangled solutions of ring-linear DNA blends," Macromolecules **55**, 1205–1217 (2022).

[21] Roovers, J., "The melt properties of ring polystyrenes," Macromolecules **18**, 1359–1361 (1985).

[22] McKenna, G. B., and D. J. Plazek, "The viscosity of blends of linear and cyclic molecules of similar molecular mass," Polymer **27**, 1368–1376 (1986).

[23] Halverson, J. D., G. S. Grest, A. Y. Grosberg, and K. Kremer, "Rheology of ring polymer melts: From linear contaminants to ring-linear blends," Phys. Rev. Lett. **108**, 038301 (2012).

[24] Parisi, D., J. Ahn, T. Chang, D. Vlassopoulos, and M. Rubinstein, "Stress relaxation in symmetric ring-linear polymer blends at low ring fractions," Macromolecules **53**, 1685–1693 (2020).

[25] Takano, A., Y. Takahashi, and Y. Matsushita, "Terminal relaxation behavior of entangled linear polymers blended with ring and dumbbell-shaped polymers in melts," Rheol. Acta **61**, 681–688 (2022).

[26] Parisi, D., M. Kaliva, S. Costanzo, Q. Huang, P. J. Lutz, J. Ahn, T. Chang, M. Rubinstein, and D. Vlassopoulos, "Nonlinear rheometry of entangled polymeric rings and ring-linear blends," J. Rheol. **65**, 695–711 (2021).

[27] Robertson, R. M., and D. E. Smith, "Strong effects of molecular topology on diffusion of entangled DNA molecules," Proc. Natl. Acad. Sci. U.S.A. **104**, 4824–4827 (2007).

[28] Chapman, C. D., S. Shanbhag, D. E. Smith, and R. M. Robertson-Anderson, "Complex effects of molecular topology on diffusion in entangled biopolymer blends," Soft Matter **8**, 9177–9182 (2012).

[29] Zhou, Y. C., C. D. Young, M. Lee, S. Banik, D. J. Kong, G. B. McKenna, R. M. Robertson-Anderson, C. E. Sing, and C. M. Schroeder, "Dynamics and rheology of ring-linear blend semidilute solutions in extensional flow: Single molecule experiments," J. Rheol. **65**, 729–744 (2021).

[30] Tsalikis, D. G., and V. G. Mavrantzas, "Size and diffusivity of polymer rings in linear polymer matrices: The key role of threading events," Macromolecules **53**, 803–820 (2020).

[31] Tsalikis, D. G., V. G. Mavrantzas, and D. Vlassopoulos, "Analysis of slow modes in ring polymers: Threading of rings controls long-time relaxation," ACS Macro Lett. **5**, 755–760 (2016).

[32] O'Connor, T. C., T. Ge, and G. S. Grest, "Composite entanglement topology and extensional rheology of symmetric ring-linear polymer blends," J. Rheol. **66**, 49–65 (2022).

[33] Peddireddy, K. R., D. Michieletto, G. Aguirre, J. Garamella, P. Khanal, and R. M. Robertson-Anderson, "DNA conformation dictates strength and flocculation in DNA-microtubule composites," ACS Macro Lett. **10**, 1540–1548 (2021).

[34] Robertson, R. M., S. Laib, and D. E. Smith, "Diffusion of isolated DNA molecules: Dependence on length and topology," Proc. Natl. Acad. Sci. U.S.A. **103**, 7310–7314 (2006).

[35] Bensafi, A., U. Maschke, and M. Benmouna, "Cyclic polymers in good solvents," Polym. Int. **49**, 175–183 (2000).

[36] Bloomfield, V., and B. H. Zimm, "Viscosity, sedimentation, et cetera, of ring-and straight-chain polymers in dilute solution," J. Chem. Phys. **44**, 315–323 (1966).

[37] Hadziioannou, G., P. M. Cotts, G. Ten Brinke, C. Han, P. Lutz, C. Strazielle, P. Rempp, and A. Kovacs, "Thermodynamic and hydrodynamic properties of dilute solutions of cyclic and linear polystyrenes," Macromolecules **20**, 493–497 (1987).

[38] Chen, Y. D., "On the ring-to-chain ratios of radii of gyration and sedimentation coefficients of polymers of the freely jointed model: Monte Carlo calculations and the ϵ method," J. Chem. Phys. **78**, 5191–5196 (1983).

[39] Tsalikis, D. G., T. S. Alexiou, P. V. Alatas, and V. G. Mavrantzas, "Conformation and diffusivity of ring and linear polyethylene oxide in aqueous solution: Molecular topology dependent concentration effects and comparison with experimental data," Macromol. Theory Simul. **29**, 2000016 (2020).

[40] Robertson, R. M., and D. E. Smith, "Self-diffusion of entangled linear and circular DNA molecules: Dependence on length and concentration," Macromolecules **40**, 3373–3377 (2007).

[41] Pan, S., D. A. Nguyen, T. Sridhar, P. Sunthar, and J. R. Prakash, "Universal solvent quality crossover of the zero shear rate viscosity of semidilute DNA solutions," J. Rheol. **58**, 339–368 (2014).

[42] Banik, S., D. J. Kong, M. J. San Francisco, and G. B. McKenna, "Monodisperse lambda DNA as a model to conventional polymers: A concentration-dependent scaling of the rheological properties," Macromolecules **54**, 8632–8654 (2021).

[43] Pan, S., D. Ahirwal, D. A. Nguyen, T. Sridhar, P. Sunthar, and J. R. Prakash, "Viscosity radius of polymers in dilute solutions: Universal behavior from DNA rheology and Brownian dynamics simulations," Macromolecules **47**, 7548–7560 (2014).

[44] Prakash, J. R., "Universal dynamics of dilute and semidilute solutions of flexible linear polymers," Curr. Opin. Colloid Interface Sci. **43**, 63–79 (2019).

[45] Zhou, Y., and C. M. Schroeder, "Dynamically heterogeneous relaxation of entangled polymer chains," Phys. Rev. Lett. **120**, 267801 (2018).

[46] MusTi, R., J.-L. Sikorav, D. Lairez, G. Jannink, and M. Adam, "Viscoelastic properties of entangled DNA solutions," C. R. Acad. Sci. Paris Ser. **320**, 599 (1995).

[47] Liu, Y. G., Y. G. Jun, and V. Steinberg, "Concentration dependence of the longest relaxation times of dilute and semi-dilute polymer solutions," J. Rheol. **53**, 1069–1085 (2009).

[48] Mason, T., A. Dhople, and D. Wirtz, "Concentrated DNA Rheology and Microrheology," in Proceedings of the 1996 MRS Fall Meeting, Boston, MA, USA, Dec. 2–6, 1996 (Materials Research Society, Pittsburgh, 1997), pp. 153–160.

[49] Pan, S., D. A. Nguyen, B. Dunweg, P. Sunthar, T. Sridhar, and J. R. Prakash, "Shear thinning in dilute and semidilute solutions of polystyrene and DNA," J. Rheol. **62**, 845–867 (2018).

[50] Chapman, C. D., K. Lee, D. Henze, D. E. Smith, and R. M. Robertson-Anderson, "Onset of non-continuum effects in microrheology of entangled polymer solutions," Macromolecules **47**, 1181–1186 (2014).

[51] Heo, Y., and R. G. Larson, "Universal scaling of linear and nonlinear rheological properties of semidilute and concentrated polymer solutions," Macromolecules **41**, 8903–8915 (2008).

[52] Teixeira, R. E., A. K. Dambal, D. H. Richter, E. S. G. Shaqfeh, and S. Chu, "The individualistic dynamics of entangled DNA in solution," Macromolecules **40**, 2461–2476 (2007).

[53] Schmidt, F. G., B. Hinner, and E. Sackmann, "Microrheometry underestimates the values of the viscoelastic moduli in measurements on F-actin solutions compared to macrorheometry," Phys. Rev. E **61**, 5646–5653 (2000).

[54] Lai, S. K., Y. Y. Wang, D. Wirtz, and J. Hanes, "Micro- and macrorheology of mucus," Adv. Drug Delivery Rev. **61**, 86–100 (2009).

[55] Ricketts, S. N., M. L. Francis, L. Farhadi, M. J. Rust, M. Das, J. L. Ross, and R. M. Robertson-Anderson, "Varying crosslinking motifs drive the mesoscale mechanics of actin-microtubule composites," Sci. Rep. **9**, 12831 (2019).

[56] Lin, Y. C., G. H. Koenderink, F. C. MacKintosh, and D. A. Weitz, "Viscoelastic properties of microtubule networks," Macromolecules **40**, 7714–7720 (2007).

[57] Laib, S., R. M. Robertson, and D. E. Smith, "Preparation and characterization of a set of linear DNA molecules for polymer physics and rheology studies," Macromolecules **39**, 4115–4119 (2006).

[58] Wen, Q., and P. A. Janmey, "Polymer physics of the cytoskeleton," Curr. Opin. Solid State Mater. Sci. **15**, 177–182 (2011).

[59] Gittes, F., B. Mickey, J. Nettleton, and J. Howard, "Flexural rigidity of microtubules and actin filaments measured from thermal fluctuations in shape," J. Cell Biol. **120**, 923–934 (1993).

[60] Hawkins, T., M. Mirigian, M. Selcuk Yasar, and J. L. Ross, "Mechanics of microtubules," J. Biomech. **43**, 23–30 (2010).

[61] Gurmessa, B., M. Francis, M. J. Rust, M. Das, J. L. Ross, and R. M. Robertson-Anderson, "Counterion crossbridges enable robust multiscale elasticity in actin networks," Phys. Rev. Res. **1**, 013016 (2019).

[62] Falzone, T. T., S. Blair, and R. M. Robertson-Anderson, "Entangled F-actin displays a unique crossover to microscale nonlinearity dominated by entanglement segment dynamics," Soft Matter **11**, 4418–4423 (2015).

[63] Chapman, C. D., and R. M. Robertson-Anderson, "Nonlinear microrheology reveals entanglement-driven molecular-level viscoelasticity of concentrated DNA," Phys. Rev. Lett. **113**, 098303 (2014).

[64] Weigand, W. J., A. Messmore, J. Tu, A. Morales-Sanz, D. L. Blair, D. D. Deheyn, J. S. Urbach, and R. M. Robertson-Anderson, "Active microrheology determines scale-dependent material properties of *Chaetopterus mucus*," PLoS One **12**, e0176732 (2017).

[65] Appleyard, D. C., K. Y. Vandermeulen, H. Lee, and M. J. Lang, "Optical trapping for undergraduates," Am. J. Phys. **75**, 5–14 (2007).

[66] Michieletto, D., P. Neill, S. Weir, D. Evans, N. Crist, V. A. Martinez, and R. M. Robertson-Anderson, "Topological digestion drives time-varying rheology of entangled DNA fluids," Nat. Commun. **13**, 4389 (2022).

[67] Tassieri, M., R. M. L. Evans, R. L. Warren, N. J. Bailey, and J. M. Cooper, "Microrheology with optical tweezers: Data analysis," New J. Phys. **14**, 115032 (2012).

[68] Squires, T. M., "Nonlinear microrheology: Bulk stresses versus direct interactions," Langmuir **24**, 1147–1159 (2008).

[69] Mason, T. G., A. Dhople, and D. Wirtz, "Linear viscoelastic moduli of concentrated DNA solutions," Macromolecules **31**, 3600–3603 (1998).

[70] Han, A., and R. H. Colby, "Rheology of entangled polyelectrolyte solutions," Macromolecules **54**, 1375–1387 (2021).

[71] Graessley, W. W., and S. F. Edwards, "Entanglement interactions in polymers and the chain contour concentration," Polymer **22**, 1329–1334 (1981).

[72] Halverson, J. D., W. B. Lee, G. S. Grest, A. Y. Grosberg, and K. Kremer, "Molecular dynamics simulation study of nonconcatenated ring polymers in a melt. I.: Statics," J. Chem. Phys. **134**, 204904 (2011).

[73] Everaers, R., S. K. Sukumaran, G. S. Grest, C. Svaneborg, A. Sivasubramanian, and K. Kremer, "Rheology and microscopic topology of entangled polymeric liquids," Science **303**, 823–826, (2004).

[74] Doi, Y., K. Matsubara, Y. Ohta, T. Nakano, D. Kawaguchi, Y. Takahashi, A. Takano, and Y. Matsushita, "Melt rheology of ring polystyrenes with ultrahigh purity," Macromolecules **48**, 3140–3147 (2015).

[75] Borger, A. *et al.*, "Threading-unthreading transition of linear-ring polymer blends in extensional flow," ACS Macro Lett. **9**, 1452–1457 (2020).

[76] Hagita, K., and T. Murashima, "Molecular dynamics simulations of ring shapes on a ring fraction in ring-linear polymer blends," Macromolecules **54**, 8043–8051 (2021).

[77] Tsalikis, D. G., and V. G. Mavrantzas, "Threading of ring poly(ethylene oxide) molecules by linear chains in the melt," ACS Macro Lett. **3**, 763–766 (2014).

[78] Katsarou, A. F., A. J. Tsamopoulos, D. G. Tsalikis, and V. G. Mavrantzas, "Dynamic heterogeneity in ring-linear polymer blends," Polymers **12**, 752 (2020).

[79] Khanal, P., K. R. Peddireddy, J. Marfai, R. McGorty, and R. M. Robertson-Anderson, "DNA topology dictates emergent bulk elasticity and hindered macromolecular diffusion in DNA-dextran composites," J. Rheol. **66**, 699–715 (2022).

[80] Fitzpatrick, R., D. Michieletto, K. R. Peddireddy, C. Hauer, C. Kyrillos, B. J. Gurmessa, and R. M. Robertson-Anderson, "Synergistic interactions between DNA and actin trigger emergent viscoelastic behavior," Phys. Rev. Lett. **121**, 257801 (2018).

[81] Michieletto, D., R. Fitzpatrick, and R. M. Robertson-Anderson, "Maximally stiffening composites require maximally coupled rather than maximally entangled polymer species," Soft Matter **15**, 6703–6717 (2019).

[82] Pelletier, V., N. Gal, P. Fournier, and M. L. Kilfoil, "Microrheology of microtubule solutions and actin-microtubule composite networks," Phys. Rev. Lett. **102**, 188303 (2009).

[83] Cox, W. P., and E. H. Merz, "Correlation of dynamic and steady flow viscosities," J. Polym. Sci. **28**, 619–622 (1958).

[84] Snijkers, F., and D. Vlassopoulos, "Appraisal of the cox-Merz rule for well-characterized entangled linear and branched polymers," Rheol. Acta **53**, 935–946 (2014).

[85] Parisi, D. *et al.*, "Nonlinear shear rheology of entangled polymer rings," Macromolecules **54**, 2811–2827 (2021).

[86] Shah, L. A., K. Gul, I. Ali, A. Khan, S. Muhammad, M. Ullah, I. Bibi, and S. Sultana, "Poly (N-vinyl formamide-co-acrylamide) hydrogels: Synthesis, composition and rheology," Iran. Polym. J. **31**, 845–856 (2022).

[87] Marion, S., N. Guillen, J. C. Bacri, and C. Wilhelm, "Acto-myosin cytoskeleton dependent viscosity and shear-thinning behavior of the amoeba cytoplasm," Eur. Biophys. J. **34**, 262–272 (2005).

[88] Khan, M., K. Regan, and R. M. Robertson-Anderson, "Optical tweezers microrheology maps the dynamics of strain-induced local inhomogeneities in entangled polymers," Phys. Rev. Lett. **123**, 038001 (2019).

[89] Peddireddy, K. R., R. Clairmont, P. Neill, R. McGorty, and R. M. Robertson-Anderson, "Optical-tweezers-integrating-differential-dynamic-microscopy maps the spatiotemporal propagation of nonlinear strains in polymer blends and composites," Nat. Commun. **13**, 5180 (2022).

[90] Huang, Q., "When polymer chains are highly aligned: A perspective on extensional rheology," Macromolecules **55**, 715–727 (2022).

[91] Ricketts, S. N., J. L. Ross, and R. M. Robertson-Anderson, "Co-entangled actin-microtubule composites exhibit tunable stiffness and power-law stress relaxation," Biophys. J. **115**, 1055–1067 (2018).

[92] See the supplementary material at https://www.scitation.org/doi/suppl/10.1122/8.0000529 for the time dependence of force trials over the course of an experiment (Fig. S1), normalized mean-squared displacements [$\pi(\tau)$] determine the linear viscoelastic moduli $G'(\omega)$ and $G''(\omega)$ (Fig. S2), and nonlinear force response of ring-linear DNA blends (0.5:0, 0.65:0) and DNA-MT composite (0.5:0.7) (Fig. S3).